

## ARTICLE OPEN



# RBM15 facilitates osimertinib resistance of lung adenocarcinoma through m6A-dependent epigenetic silencing of SPOCK1

Hongxiang Li<sup>1,2,10</sup>, Yin Li<sup>3,10</sup>, Xiaoxiao Zheng<sup>4</sup>, Fangqian Chen<sup>5</sup>, Shufen Zhang<sup>4</sup>, Shuguang Xu<sup>6</sup>, Yinyu Mu<sup>1</sup>, Wei Shen<sup>7</sup>, Jingtao Tong<sup>6</sup>, Hang Chen<sup>1</sup>, Zeyang Hu<sup>1,2</sup>, Jiaheng Zhang<sup>1,2</sup>, Keyue Qiu<sup>1,2</sup>, Wei Chen<sup>8,9</sup>, Xinghua Cheng<sup>3</sup> and Guodong Xu<sup>1,2</sup>

© The Author(s) 2024

Lung cancer is the leading cause of cancer-related mortality globally. N6-methyladenosine (m6A) is the most abundant modification in mammalian mRNA and is involved in the biological regulation of tumors, including lung cancer. However, the role of m6A-related proteins, such as RNA-binding motif protein 15 (RBM15), in lung cancer progression remains largely unknown. Our study indicated that RBM15 is significantly overexpressed in lung adenocarcinoma, serving as an independent prognostic factor for poor outcomes and facilitating tumor cell proliferation and migration. RBM15 was markedly elevated in patients with EGFR mutations, correlating with a poorer prognosis, while it had negligible prognostic value in EGFR wild-type patients. As EGFR-tyrosine kinase inhibitors (TKIs) are the standard treatment for patients with EGFR mutations, we subsequently determined that RBM15 drives osimertinib resistance via a novel mechanism: enhancing m6A modification of cwc- and kazal-like domains proteoglycan 1 (SPOCK1) mRNA, promoting epithelial–mesenchymal transition-mediated osimertinib resistance through a bypass activation pathway. These findings were validated in osimertinib-resistant H1975 cells and organoids from patients with osimertinib-resistant lung adenocarcinoma. Furthermore, the RBM15–SPOCK1 axis was activated in drug-tolerant persister cells, indicating that early targeting of RBM15 during EGFR-TKI treatment could dramatically extend the patient response and benefit from TKI therapy. Our results emphasize the critical role of RBM15 in reversing EGFR-TKI resistance and propose it as a promising therapeutic target for prolonging TKI treatment benefits in patients with lung adenocarcinoma.

*Oncogene*; <https://doi.org/10.1038/s41388-024-03220-z>

## HIGHLIGHTS

- RBM15 regulates the sensitivity of EGFR-mutant lung adenocarcinoma to osimertinib.
- RBM15 binds to SPOCK1 mRNA and inhibits its expression through an m6A-mediated mechanism.
- Knockdown of RBM15 enhances the sensitivity of resistant cells and resistant organoids to osimertinib by upregulating SPOCK1 expression.
- The RBM15–SPOCK1 axis promotes epithelial–mesenchymal transition-mediated osimertinib resistance through a bypass activation pathway.
- The RBM15–SPOCK1–EMT axis is activated early during osimertinib treatment, rather than during the advanced stage of tumor resistance.

## INTRODUCTION

Lung cancer remains a deadly cancer globally, with a 5-year survival rate of 10–20% in most regions, and its incidence continues to rise [1]. Non-small cell lung cancer (NSCLC) accounts for 85% of all cases, with lung adenocarcinoma (LUAD) comprising 53.3% of NSCLC cases [2]. Despite diagnosis and treatment pathway advancements, 85% of patients are diagnosed at an advanced stage [3]. Consequently, there is a critical need to explore the lung cancer onset and progression mechanisms.

N6-methyladenosine (m6A) is the most abundant modification in mammalian mRNA [4] and is dynamically regulated by “writers”, “erasers”, and “readers” (collectively known as WERs) [5]. m6A is involved in the biological processes of diseases such as osteosarcoma

<sup>1</sup>Department of Thoracic Surgery, The Affiliated Lihuili Hospital of Ningbo University, Ningbo, Zhejiang, China. <sup>2</sup>Health Science Center, Ningbo University, Ningbo, Zhejiang, China. <sup>3</sup>Department of Oncology, Shanghai Chest Hospital, Shanghai Jiao Tong University School of Medicine, Shanghai, China. <sup>4</sup>Cancer Institute of Integrated Traditional Chinese and Western Medicine, Key Laboratory of Cancer Prevention and Therapy Combining Traditional Chinese and Western Medicine of Zhejiang Province, Zhejiang Academy of Traditional Chinese Medicine, Tongde Hospital of Zhejiang Province, Hangzhou, Zhejiang, China. <sup>5</sup>Department of Gastrointestinal Surgery, The Lihuili Affiliated Hospital, Ningbo University, Ningbo, Zhejiang, China. <sup>6</sup>Department of Respiratory, The Lihuili Affiliated Hospital, Ningbo University, Ningbo, Zhejiang, China. <sup>7</sup>Department of Pulmonary and Critical Care Medicine, The Third People's Hospital of Cixi, Ningbo, Zhejiang, China. <sup>8</sup>Department of General Surgery, Sir Run Run Shaw Hospital, School of Medicine, Zhejiang University, Hangzhou, Zhejiang, China. <sup>9</sup>Key Laboratory for Accurate Diagnosis and Treatment of Abdominal Infection in Zhejiang Province, Sir Run Run Shaw Hospital, School of Medicine, Zhejiang University, Hangzhou, Zhejiang, China. <sup>10</sup>These authors contributed equally: Hongxiang Li, Yin Li. ✉email: [weichen1982zju@gmail.com](mailto:weichen1982zju@gmail.com); [xinhua.cheng@sjtu.edu.cn](mailto:xinhua.cheng@sjtu.edu.cn); [xuguodong@nbu.edu.cn](mailto:xuguodong@nbu.edu.cn)

Received: 30 July 2024 Revised: 29 October 2024 Accepted: 1 November 2024

Published online: 11 November 2024

[6], ovarian cancer [7], bladder tumors [8], and breast cancer [9]. The writers are part of a methyltransferase complex that catalyzes the m6A modification, influencing mRNA stability, turnover, localization, and translation efficiency [10]. We determined that RNA-binding motif protein 15 (RBM15) is a key WER with significant diagnostic and therapeutic potential in LUAD and profoundly affects cellular behavior, proliferation, and migration capabilities in vivo. RBM15 is a member of the SPEN (Split-end) family of proteins [11], which function as writers and are oncogenic factors in laryngeal squamous cell carcinoma [12] and pancreatic cancer [13]. Furthermore, RBM15 is highly expressed in lung cancer, promoting ferroptosis by modulating the TGF- $\beta$ -Smad2 pathway [14]. Our statistical results did not confirm a correlation between RBM15 expression and tumor size or clinical characteristics, prompting us to investigate the role of RBM15 in LUAD. We observed that RBM15 expression was significantly increased in patients with *EGFR* mutations and was closely associated with prognosis. However, no significant correlation was found between RBM15 expression and prognosis in *EGFR* wild-type patients.

*EGFR* mutations are the most prevalent in LUAD, with exon 19 deletions (del19) and point mutations in exon 21 (L858R) representing typical mutations accounting for ~80–85% of *EGFR* mutations [15]. First- and second-generation *EGFR* tyrosine kinase inhibitors (*EGFR*-TKIs) are the standard treatments for del19 and L858R mutations and are widely used clinically. However, resistance due to secondary mutations such as *EGFR* T790M has limited their clinical utility. Third-generation TKIs, exemplified by osimertinib, target the T790M mutation and offer high efficacy and favorable outcomes, with a median progression-free survival (PFS) and median overall survival (OS) of 18.9 and 38.6 months, respectively, becoming the preferred first-line treatment in clinical settings [16–19].

We determined that overexpressing RBM15 decreased drug sensitivity in osimertinib-sensitive cells. Consequently, patients with high-RBM15 expression had shorter PFS when treated with osimertinib. Therefore, we hypothesized that RBM15 promotes the development of *EGFR*-TKI resistance. Osimertinib treatment resistance inevitably emerges and exhibits heterogeneity. The mechanisms of acquired resistance primarily include *EGFR*-dependent resistance (usually secondary *EGFR* mutations such as the C797S mutation) and *EGFR*-independent resistance (mainly *MET* amplification, epithelial–mesenchymal transition [EMT], small cell transformation) [20–22]. Although combined TKI and *MET* inhibitor treatment improves the efficacy against TKI-refractory tumors when *EGFR* mutation coexists with *MET* amplification [23], the heterogeneous resistance mechanisms often leave many *EGFR*-independent resistance mechanisms without specific treatments. Additionally, the immune checkpoint inhibitor (ICI) therapy outcomes in patients with *EGFR* mutations have been disappointing [20], necessitating further exploration into resistance mechanisms to seek more effective treatment strategies.

In this investigation, we established RBM15 overexpression in LUAD, notably in cases with *EGFR*-TKI resistance. SPOCK1 (cwc- and kazal-like domains proteoglycan 1) acts as a downstream effector of RBM15. RBM15 enhanced the m6A modification of *SPOCK1* mRNA, inhibiting its expression and activating EMT, inducing osimertinib resistance through a bypass activation mechanism. Additionally, we determined that the RBM15–SPOCK1–EMT axis is activated early in drug-tolerant persister cells (DTPCs), indicating that targeting RBM15 could be a promising strategy to reverse *EGFR*-TKI resistance and prolong the therapeutic benefits of TKIs.

## RESULTS

### RBM15 overexpression in LUAD enhances malignant progression and predicts poor prognosis

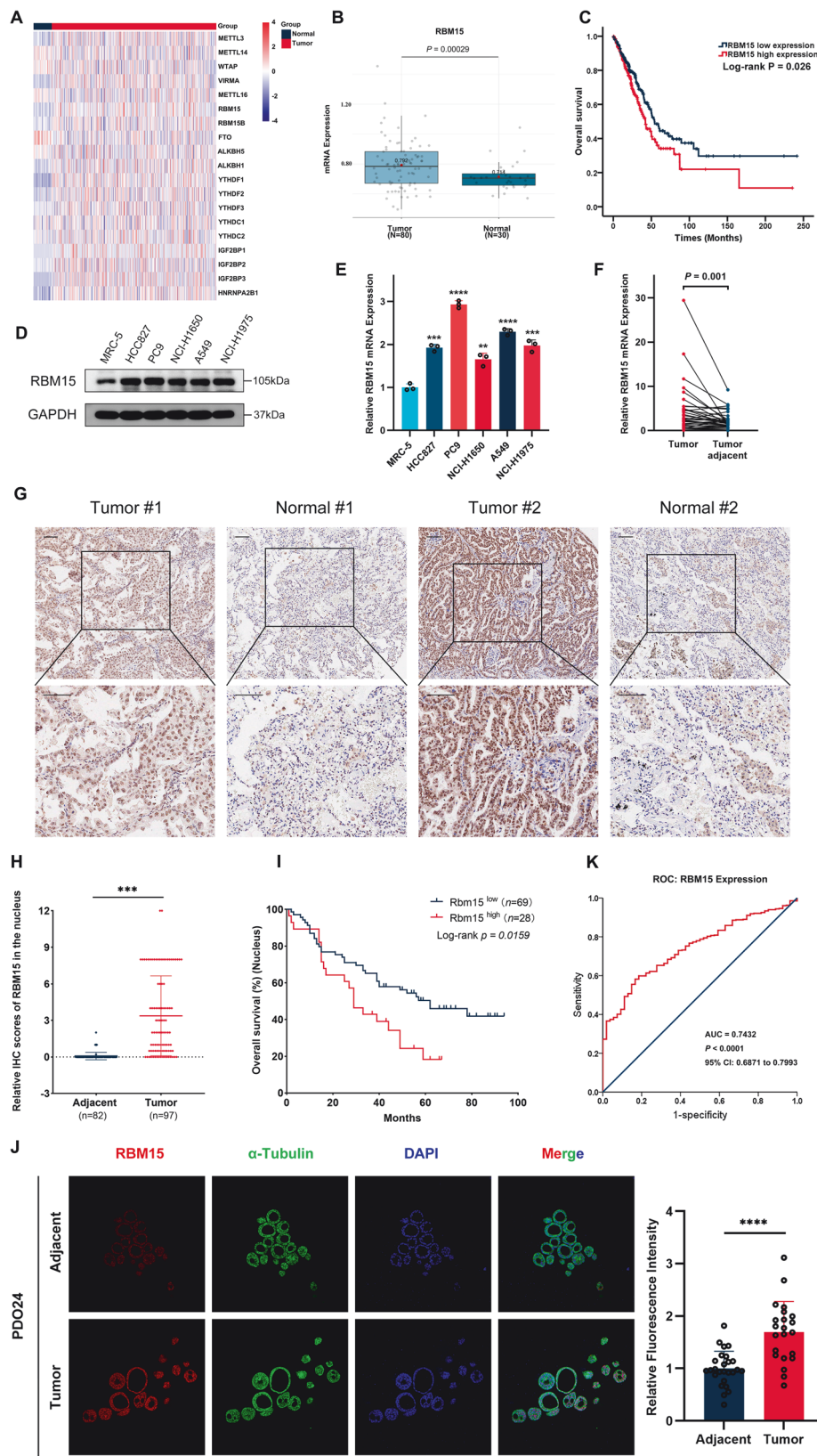
We investigated the functional implications of m6A-related genes in LUAD by examining the expression profiles of m6A-associated

genes, encompassing m6A WERs, within The Cancer Genome Atlas (TCGA)-LUAD dataset. The analysis identified dysregulation in the expression of 15 WER genes (Fig. 1A). The expression levels of these genes were corroborated in the GSE43458 dataset through the online platform Lung Cancer Explorer (<https://lce.biohpc.swmed.edu/lungcancer/>), which substantiated significant *RBM15*, *YTHDF1*, *IGF2BP1*, *IGF2BP3*, and *HNRNPA2B1* upregulation in LUAD samples relative to normal tissues, alongside marked *METTL14* and *FTO* downregulation (Fig. 1B and Fig. S1A–F). Furthermore, we explored the association between the expression of these genes and OS in patients with LUAD using The Human Protein Atlas (THPA, <https://www.proteinatlas.org/>) data. The results indicated that elevated RBM15 and HNRNPA2B1 expression predicted reduced survival durations (Fig. 1C and Fig. S1G).

These observations prompted further investigation of RBM15 function in LUAD. The LUAD cell lines demonstrated elevated RBM15 protein and mRNA levels compared to the MRC-5 cells (Fig. 1D, E). The insights from the bioinformatics analysis and in vitro cellular assays were substantiated using tumor and adjacent non-tumor tissues from 40 patients. qRT-PCR confirmed the significantly enhanced RBM15 expression in the tumor samples (Fig. 1F), which was validated by IHC staining of a TMA cohort (Fig. 1G, H). The writing of m6A primarily occurs in the nucleus, where it is incorporated into mRNA in a co-transcriptional manner, and then exported to the cytoplasm. Therefore, we focused our attention on the expression of RBM15 in the nucleus [24]. Despite being categorized as a nuclear protein, the presence of RBM15 in the nuclear and cytoplasmic fractions of the tumor and adjacent tissues prompted our analysis of its expression separately in these compartments, which revealed consistently elevated RBM15 levels in tumor tissues across both compartments (Fig. 1H and Fig. S1H). Kaplan–Meier survival analysis indicated that elevated RBM15 expression correlated with poor OS (Fig. 1I and Fig. S1I), validating TPHA analytical outcomes. Furthermore, multivariate analysis identified cytoplasmic RBM15 protein expression as an independent prognostic factor for patient outcomes (Table 1).

PDOs are highly faithful in vitro preclinical models [25] and were used to construct organoids derived from LUAD and matched adjacent tissues. Immunofluorescent semi-quantitative analysis confirmed the RBM15 overexpression in the LUAD-derived organoids (Fig. 1J). The receiver operating characteristic (ROC) curves revealed that RBM15 expression demonstrated moderate sensitivity (0.582) and high specificity (0.883) for the clinical diagnosis of LUAD (Fig. 1K). Collectively, these results establish that RBM15 is overexpressed in LUAD and intricately linked with adverse prognostic implications.

The role of RBM15 in LUAD was elucidated using siRNAs and overexpression plasmids for RBM15 knockdown in A549 and PC9 cells and RBM15 overexpression in HCC827 and NCI-H1975 cells, respectively (Fig. S2A–D). RBM15 is key in methylation modification [5], and we analyzed m6A methylation in cells with altered RBM15 using a quantification kit, detecting decreased m6A levels after RBM15 knockdown and increased levels after RBM15 overexpression (Figs. S3A and S4A). CCK-8 and EdU assays revealed that RBM15 overexpression enhanced proliferation, while knockdown reduced it (Figs. S3B–E and S4B–E). The Transwell assays indicated enhanced migration and invasion with RBM15 overexpression, and opposite effects upon knockdown (Figs. S3F, G and S4F, G). The lentiviral vectors established stable RBM15 modulation in the PDOs (Fig. S2E–H). After 7 days, the organoids with RBM15 overexpression demonstrated more proliferation, while knockdown reduced proliferation (Fig. S4H, I). RBM15 knockdown in H1975 cells used to create xenografts in nude mice (Fig. S2I, J) significantly reduced tumor volumes (Fig. S4J–L). Ki-67 staining confirmed weaker proliferation in the sh-RBM15 group (Fig. S4M, N). Accordingly, we propose that RBM15 contributes to LUAD tumorigenesis.



### RBM15 upregulation in EGFR-mutant LUAD predicts poor prognosis and lower TKI sensitivity

We examined the relationship between RBM15 expression and the clinical features of patients in a TMA cohort. The clinical statistical

analysis indicated that the RBM15 cytoplasmic and nuclear protein levels did not correlate with the patient's age, sex, or tumor stage (Tables S5 and S6), indicating the need for further research to interpret these results. A detailed exploration of clinical

**Fig. 1 RBM15 expression in LUAD highlights its potential as a prognostic indicator.** **A** Expression heatmap of TCGA-LUAD dataset m6A WERs. **B** Comparison of *RBM15* mRNA levels between GSE43458 LUAD tissues ( $n = 80$ ) and normal lung tissues ( $n = 30$ ). Mann–Whitney test. **C** Kaplan–Meier survival curves showing OS in patients with LUAD stratified by *RBM15* expression using TCGA data. **D** Western blot analysis quantifying *RBM15* protein levels. **E** qRT-PCR assessment of *RBM15* mRNA in cell lines. *T* test. **F** qRT-PCR detection of *RBM15* mRNA expression in paired LUAD tissues ( $n = 40$ ). Based on the aforementioned big data analysis, we believe that 40 paired samples are sufficient to ensure the reproducibility of the experiment. Wilcoxon test. **G, H** IHC staining of *RBM15* in LUAD tissue sections ( $n = 97$ ) and adjacent non-tumor lung tissue ( $n = 82$ ) from a TMA cohort. Representative images and IHC scoring are shown (scale bar: 100  $\mu$ m).  $\chi^2$  test. **I** Kaplan–Meier analysis correlating *RBM15* expression with OS in the LUAD TMA cohort. **J** Immunofluorescence staining of *RBM15* in patient-derived LUAD organoids vs. normal tissue organoids (scale bar: 50  $\mu$ m). *T* test. **K** ROC curve analysis evaluating the diagnostic performance of *RBM15* with a sensitivity of 0.582 and specificity of 0.883, derived from TCGA data. Error bars represent the means  $\pm$  SDs. \*\* $P < 0.01$ , \*\*\* $P < 0.001$ , \*\*\*\* $P < 0.0001$ .

**Table 1.** Univariate and multivariate analyses of the factors correlated with overall survival of lung adenocarcinoma patients.

Variables	Univariate analysis			Multivariate analysis		
	HR	95% CI	<i>p</i> value	HR	95% CI	<i>p</i> value
RBM15 expression (cytoplasm)	1.937	1.1050–3.396	0.021*	2.222	1.054–4.682	0.036*
RBM15 expression (nucleus)	1.925	1.113–3.328	0.019*	0.710	0.562–2.328	0.710
Sex	1.112	0.654–1.891	0.695			
Grade	1.090	0.637–1.863	0.753			
Age	1.653	0.979–2.792	0.060			
T stage	1.692	1.127–2.539	0.011*	1.053	0.529–2.096	0.884
N stage	1.956	1.503–2.546	<0.001*	1.584	0.943–2.660	0.082
TNM stage	1.993	1.448–2.744	<0.001*	1.268	0.587–2.739	0.545

\*Statistically significant ( $p < 0.05$ ).

characteristics within the TMA cohort revealed that nuclear *RBM15* expression was markedly higher in the patients with *EGFR* mutations than those without (Fig. 2A, B). This observation was confirmed using immunofluorescence assessment of *RBM15* expression in the PDOs with and without *EGFR* mutations. As expected, the PDOs with mutations had elevated *RBM15* levels (Fig. 2C, D), prompting speculation of a potential unique role for *RBM15* in *EGFR*-mutant tumors. The hypothesis was explored by stratifying TCGA-LUAD *EGFR*-mutant patient samples into two groups based on the median *RBM15* expression level (high and low). The prognostic significance of *RBM15* expression levels was assessed using Kaplan–Meier survival curves, which revealed a statistically significant reduction in OS in the high-expression cohort (Fig. 2E). Conversely, no statistically significant correlation was observed between *RBM15* expression and OS in the patients without *EGFR* mutations (Fig. S5A). These results underscore a potential interaction between *RBM15* expression and *EGFR* mutation status, which may profoundly affect LUAD clinical outcomes. This interaction warrants a deeper exploration of the mechanistic pathways that could mediate these effects.

As *EGFR*-TKIs are the frontline therapy for *EGFR*-mutant NSCLC [26], we investigated whether *RBM15* affected *EGFR*-TKI therapeutic efficacy. As we lacked TCGA *EGFR*-TKI treatment data, we analyzed pre- and post-resistance *EGFR*-TKI RNA-seq data from patient tissues collected prospectively by Roper et al. [27]. We determined that patients with higher pre-treatment *RBM15* expression had shorter PFS durations (9.53 vs. 12.63 months) (Fig. 2F). Despite finding a *P* value of 0.197 through statistical analysis, we acknowledged that this result might have been influenced by small sample size. Nevertheless, these findings provided valuable insights into the potential correlation between *RBM15* expression and *EGFR*-TKI sensitivity, prompting further investigation. Based on these findings, we obtained TCGA *EGFR*-TKI sensitivity data using oncoPredict [28], stratifying patients according to median *RBM15* expression (low and high). The analysis demonstrated that the high-*RBM15* expression group exhibited relatively higher *EGFR*-TKI  $IC_{50}$  values (Fig. S5B, S5C). The

osimertinib-sensitive H1975 cells (harboring *EGFR* T790M) and HCC827 cells (harboring *EGFR* L858R) were transfected with a control vector or *RBM15* overexpression plasmid. *RBM15* overexpression significantly increased the  $IC_{50}$  in the HCC827 cells ( $IC_{50} = 0.094 \mu$ M vs.  $0.475 \mu$ M) and H1975 cells ( $IC_{50} = 0.818 \mu$ M vs.  $6.95 \mu$ M) (Fig. 2G, H). The results indicated that *RBM15* has greater biological significance and is associated with *EGFR*-TKI sensitivity in *EGFR*-mutant LUAD.

### **RBM15 is critical in mediating osimertinib resistance**

TCGA drug sensitivity data were validated by establishing H1975-OR cells. The H1975-OR cells exhibited an  $IC_{50}$  of  $13.92 \mu$ M compared to  $0.66 \mu$ M in the parental cells (Fig. 3A), demonstrating stable osimertinib resistance. Proliferation, migration, and invasion signaling pathway activation in *EGFR*-mutant NSCLC depends on *EGFR* dimerization and tyrosine kinase activation within the intracellular domains, which phosphorylates intracellular molecules [29]. *EGFR* phosphorylation and changes in downstream oncogenic pathways in H1975-OR cells treated for 48 h with  $10 \mu$ M osimertinib were compared using western blotting. The results confirmed that osimertinib significantly reduced phosphorylated (p)-*EGFR* levels. While the p-ERK results indicated that the ERK pathway was notably inhibited, osimertinib did not suppress the protein kinase B (AKT) signaling pathway (Fig. 3B). This result suggested that the H1975-OR cells might have *EGFR*-independent resistance mechanisms, potentially using alternate inputs from the phosphatidylinositol 3-kinase (PI3K)–AKT signaling pathway for survival. Considering TCGA drug sensitivity results (Fig. S5B, C), *RBM15* expression levels in the H1975-OR cells were assessed using western blotting and qRT-PCR, which demonstrated higher *RBM15* mRNA and protein expression levels in the H1975-OR cells than the parental H1975 cells (Fig. 3B), corroborating our conclusions.

Knocking down *RBM15* expression in H1975-OR cells (Fig. S2K, L) significantly enhanced osimertinib sensitivity ( $IC_{50} = 9.51 \mu$ M vs.  $1.545 \mu$ M and  $1.34 \mu$ M) (Fig. 3E). Results more closely aligned with clinical patient outcomes were obtained by collecting lung biopsy



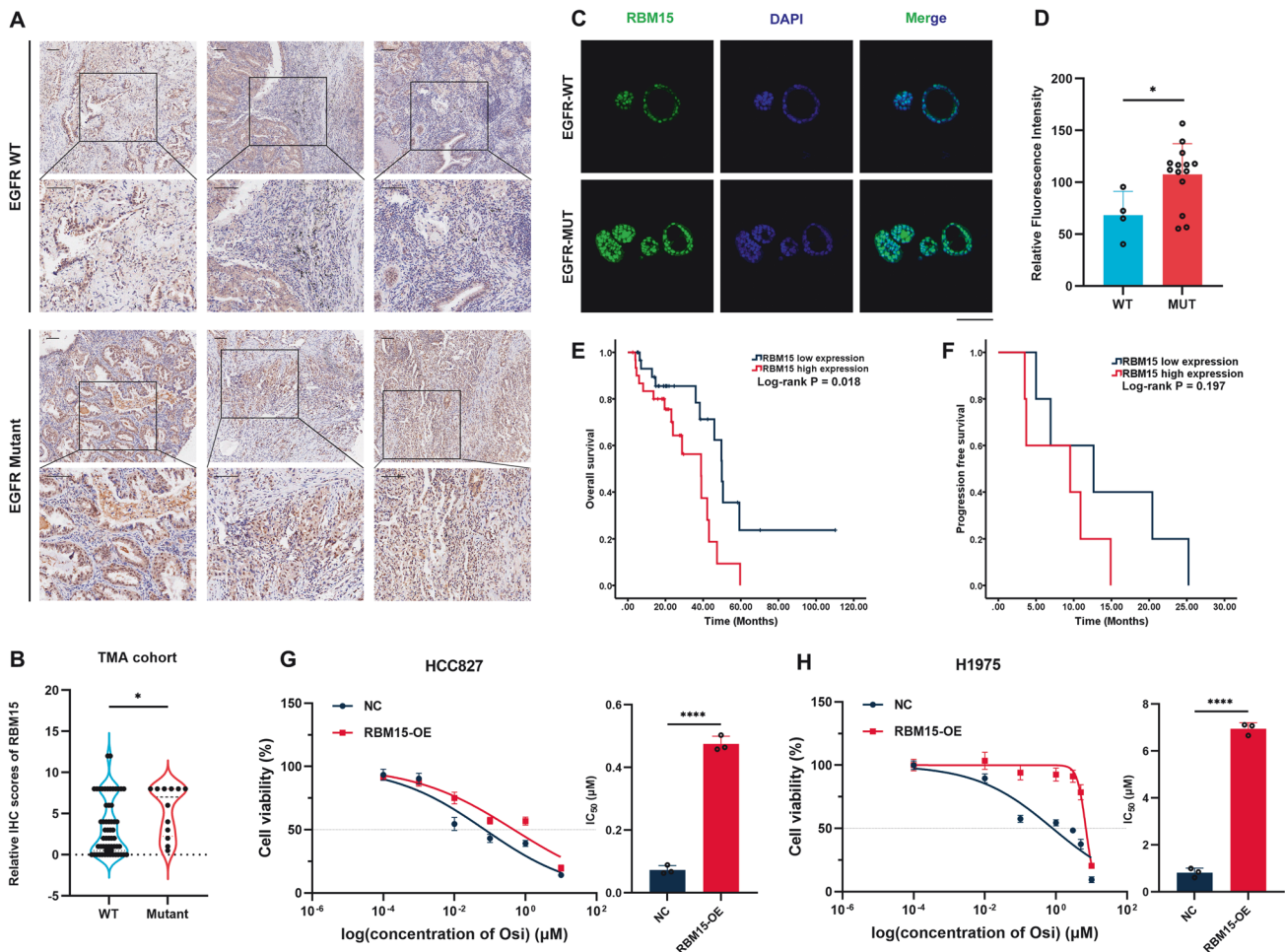


**Fig. 2** Elevated RBM15 expression in patients with LUAD with EGFR mutations correlates with adverse outcomes. **A, B** Representative image of IHC staining and IHC scores of RBM15 from EGFR wild-type (WT) or mutant patients. Mann–Whitney test. **C, D** Immunofluorescence of RBM15 protein expression in LUAD PDO with or without EGFR mutations (scale bar: 50  $\mu$ m). *T* test. **E** OS in TCGA LUAD cases with EGFR mutation according to RBM15 expression. **F** PFS after initiation of osimertinib treatment in patients with EGFR mutations expressing high vs. low RBM15 mRNA levels. **G, H** Osimertinib  $IC_{50}$  value of HCC827 and H1975 cells transfected with NC and RBM15-OE. *T* test. Error bars represent the means  $\pm$  SDs. \* $P < 0.05$ , \*\*\*\* $P < 0.0001$ .

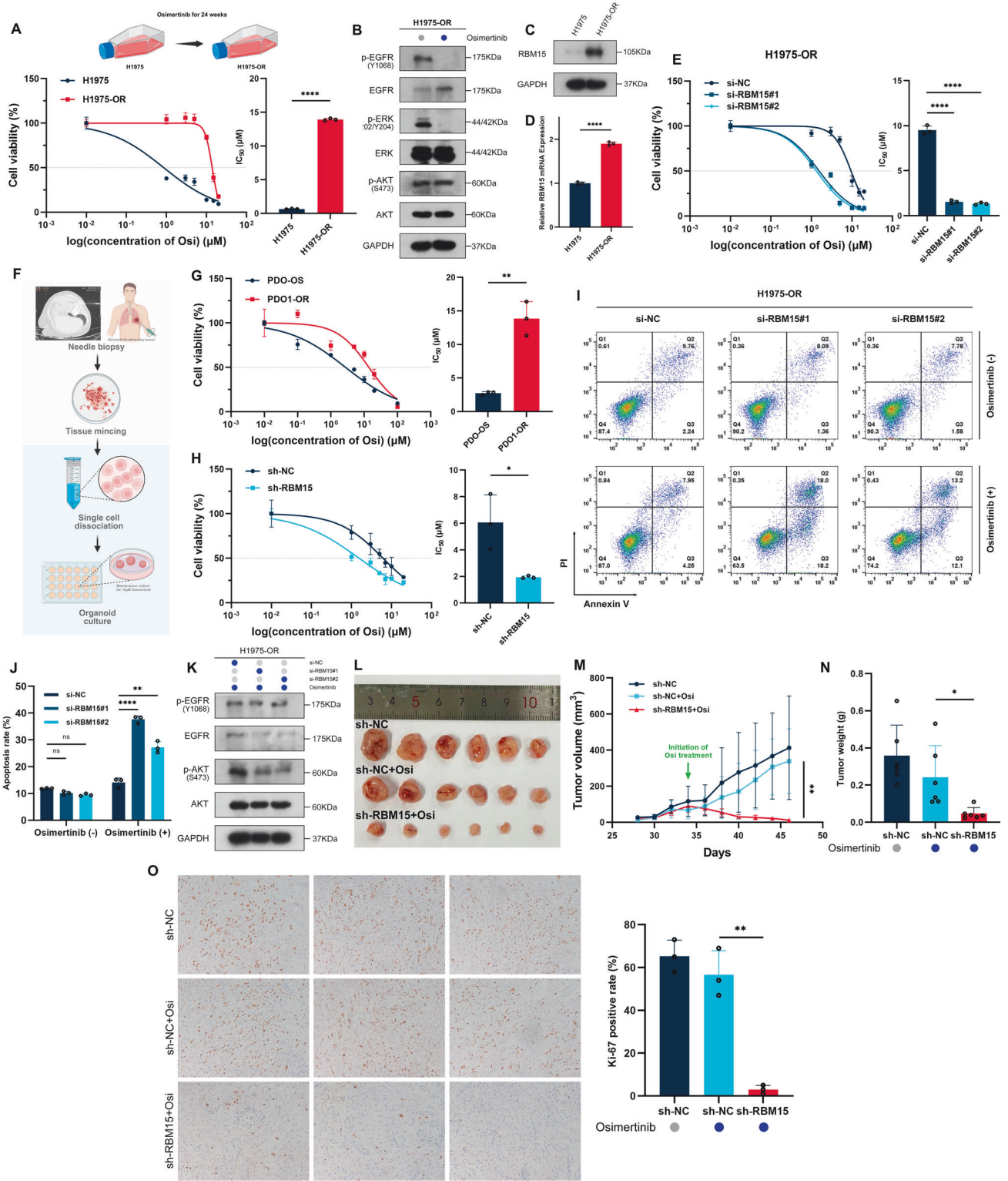
tumor samples from patients with LUAD with EGFR-TKI-refractory disease and successfully establishing a patient-derived LUAD organoid, PDO1-OR (Fig. 3F). Hematoxylin–eosin (H&E) and IHC staining confirmed that PDO1-OR demonstrated typical adenocarcinoma characteristics (Fig. S5D, E). Following osimertinib selection and validation, PDO1-OR demonstrated greater resistance than EGFR-TKI-naïve organoids ( $IC_{50} = 2.747 \mu$ M vs.  $13.86 \mu$ M) (Fig. 3G and Fig. S5F). Additionally, stable knockdown of RBM15 in PDO1-OR (Fig. S2M, N) suggested that lower RBM15 expression indicated increased osimertinib sensitivity ( $IC_{50} = 6.064 \mu$ M vs.  $1.947 \mu$ M) (Fig. 3H). Flow cytometry assessment of apoptosis post-RBM15 silencing revealed that RBM15 knockdown had a negligible impact on apoptosis in the absence of osimertinib. However, 48-h osimertinib treatment significantly increased apoptosis in the knockdown group (Fig. 3I, J) and markedly suppressed p-AKT levels (Fig. 3K). These results indicated that downregulating RBM15 expression did not directly trigger apoptosis; instead, it increased the sensitivity to osimertinib, enhancing cell death.

Subsequently, we injected H1975-OR cells stably transfected with sh-NC or sh-RBM15 subcutaneously into nude mice. The mice were treated orally with osimertinib mesylate once the tumors reached  $\sim 5$  mm in diameter. While osimertinib alone did not significantly reduce tumor volumes, combining osimertinib with

sh-RBM15 substantially suppressed tumor growth (Fig. 3L–N). Ki-67 staining highlighted significantly reduced xenograft tumor proliferation following the combined treatment (Fig. 3O). Accordingly, these results indicated that RBM15 is critical in sustaining the survival of EGFR-TKI-resistant cells during osimertinib treatment.

### RBM15 silences SPOCK1 expression in an m6A-dependent manner

The molecular mechanisms by which RBM15 functions were examined using RNA-seq to identify transcriptional changes following RBM15 knockdown, which identified 97 potential downstream targets ( $|\log_2$  fold change  $\geq 1.2$ ,  $P \leq 0.01$ , Table S7). The investigation progressed using MeRIP-seq to examine m6A enrichment on RNA post-RBM15 overexpression, which revealed 6577 new m6A peaks predominantly near stop codons (Fig. 4B and Table S8), with GGACH as the most frequent motif (Fig. 4C). Intersecting both datasets yielded 16 candidate genes (Fig. 4A), which we validated using qRT-PCR. The analysis confirmed a significant correlation consistent with the sequencing results for SPOCK1 and IL411 under RBM15 silencing and overexpression scenarios (Fig. 4D, E and Fig. S6A, B). Given its pronounced correlation, we conducted an in-depth investigation into the function of SPOCK1. The western blotting revealed that



manipulating RBM15 in HCC827 and H1975 cells significantly affected SPOCK1 protein levels (Fig. 4F, G).

Potential protein-level direct interactions between RBM15 and SPOCK1 were investigated using an IP experiment, which revealed no substantive evidence of protein–protein interaction (Fig. S6C). Subsequently, the interaction between RBM15 protein and SPOCK1 mRNA was examined using RIP assays utilizing antibodies against RBM15 and m6A. The qRT-PCR results indicated significant

enrichment of SPOCK1 mRNA bound to both antibodies compared to the IgG control. Notably, RBM15 overexpression enhanced m6A accumulation on SPOCK1 mRNA (Fig. 4H, I). This interaction suggested a regulatory effect of RBM15 on SPOCK1 mRNA regulation were validated by suppressing methylation modifications of cellular RNA using the methylation inhibitor DAA (Fig. 4J). The analysis demonstrated that reducing m6A levels

**Fig. 3 RBM15 suppression augments osimertinib sensitivity in resistant LUAD models.** **A** H1975 cells were exposed to increasing concentrations of osimertinib and cultured for 24 weeks to select H1975-OR cells (top panel). H1975 and H1975-OR cells were incubated with osimertinib for 48 h, cell viability was measured using the CCK-8 assay, and the  $IC_{50}$  was calculated (bottom panel). *T* test. **B** Western blot investigation of EGFR, ERK, and AKT protein levels and their phosphorylation. **C, D** RBM15 protein and mRNA expression levels in H1975 and H1975-OR were assessed using western blot and qRT-PCR. *T* test. **E** Osimertinib  $IC_{50}$  of H1975-OR cells transfected with si-NC, si-RBM15#1, or si-RBM15#2. *T* test. **F** A schematic diagram for the construction of drug-resistant organoids. **G** PDO1-OR and osimertinib-sensitive organoids were incubated with osimertinib for 48 h, cell viability was measured using the CCK-8 assay, and the  $IC_{50}$  was calculated. *T* test. **H** Osimertinib  $IC_{50}$  value of PDO1-OR transfected with sh-NC or sh-RBM15. *T* test. **I, J** Effects of RBM15 knockdown on H1975-OR and PDO1-OR apoptosis assessed using flow cytometry and TUNEL staining. *T* test. **K** Western blot analysis of EGFR and AKT proteins and their phosphorylation levels after knockdown of RBM15 and 48-h osimertinib treatment. **L** Representative images of xenograft tumors from sh-NC, sh-NC + Osi, and sh-RBM15 + Osi groups. **M, N** Tumor growth curve and tumor weights. *T* test. **O** Representative images of Ki-67 positive staining in xenografted tumors. *T* test. Error bars represent the means  $\pm$  SDs. \**P* < 0.05, \*\**P* < 0.01, \*\*\*\**P* < 0.0001.

substantially increased *SPOCK1* mRNA expression (Fig. 4K), highlighting the critical role of m6A in modulating mRNA stability and expression.

The data suggested that RBM15 silences *SPOCK1* expression through an m6A-dependent mechanism.

#### **SPOCK1 acts as a downstream factor and reverses the RBM15 knockdown-induced osimertinib sensitivity**

Considering these experimental outcomes, we posited that RBM15-induced osimertinib resistance might be mediated through its interaction with *SPOCK1*. The hypothesis was examined using western blotting and qRT-PCR to measure the *SPOCK1* protein and mRNA levels in H1975-OR cells compared to the parental cell line. The analyses demonstrated significantly reduced *SPOCK1* in the H1975-OR cells (Fig. 4L, M). Subsequently, RBM15 was stably knocked down in H1975-OR cells and PDO1-OR using lentiviral vectors (Fig. S2I, J, M, N), which increased *SPOCK1* protein and mRNA levels (Fig. S2Q, R), confirming a linked expression pattern in the resistant cells and organoid models. The  $IC_{50}$  assays revealed that inhibiting RBM15 in H1975-OR cells substantially increased their susceptibility to osimertinib ( $IC_{50}$  = 6.404  $\mu$ M vs. 3.439  $\mu$ M). Furthermore, concurrent knockdown of *SPOCK1* under these conditions reversed osimertinib resistance ( $IC_{50}$  = 3.439  $\mu$ M vs. 7.306  $\mu$ M) (Fig. 4N). Parallel findings were documented in PDO1-OR (Fig. 4O). Furthermore, knocking down *SPOCK1* mitigated the RBM15 knockdown-augmented apoptotic activity following osimertinib treatment (Fig. 4P, Q). These results strongly supported the notion that *SPOCK1* is a critical downstream mediator that reverses the osimertinib resistance attributed to RBM15.

#### **RBM15 confers osimertinib resistance by EMT phenotype**

The mechanisms of osimertinib resistance have been extensively investigated and include *EGFR*-dependent (on-target) and *EGFR*-independent (off-target) resistance pathways [29]. The resistance mechanisms in H1975-OR cells were examined using whole-exome sequencing (WES), which did not detect mutations associated with third-generation *EGFR*-TKI resistance (Table S9). Despite harboring the *EGFR* T790M mutation, our analysis integrating WES data with drug sensitivity assays revealed that the H1975-OR cells exhibited insensitivity to osimertinib, suggesting the presence of *EGFR*-independent resistance mechanisms.

The underlying mechanisms were further examined using RNA-seq to analyze gene expression profiles and enrichment in H1975-OR cells. The control was the parental cells. Differentially expressed genes (DEGs) between the two cell populations underwent enrichment analysis (Fig. S6F). The gene set enrichment analysis (GSEA) results were visualized using ridge-line plots, which indicated significant enrichment of EMT pathways in the H1975-OR cells (Fig. 5A, B). A volcano plot revealed upregulated mesenchymal markers (VIM, AXL), down-regulation of the epithelial marker CDH1, and markedly

increased expression of the genes encoding EMT transcriptional regulators (ZEB1, ZEB2) (Fig. 5C).

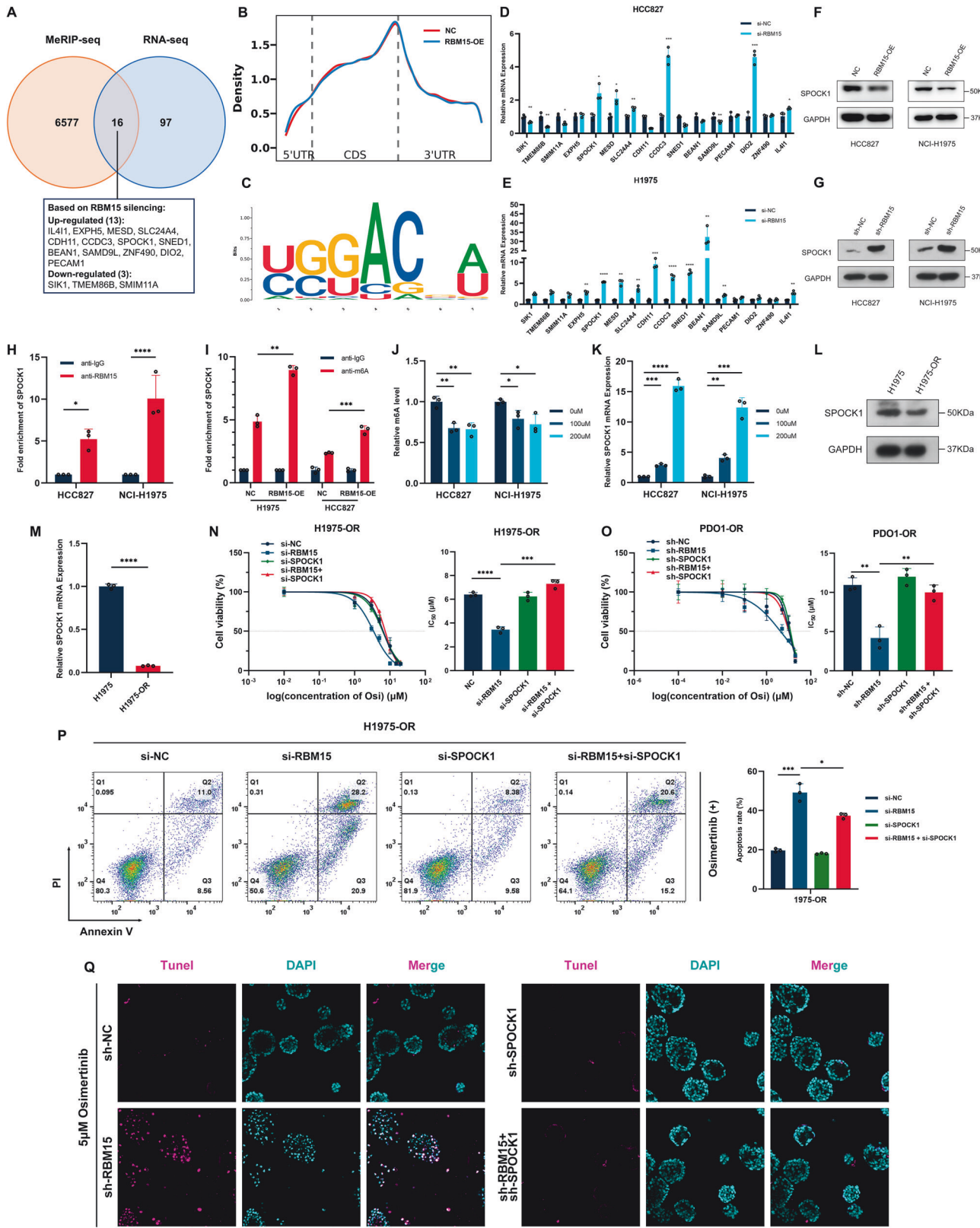
As EMT is a key pathway in *EGFR*-TKI resistance [30], and notably, the overexpression of the EMT transcriptional regulator ZEB1 induces resistance in *EGFR*-mutant NSCLC [31], we investigated the cellular morphology of H1975-OR cells. Compared to the parental H1975 cells, the H1975-OR cells appeared larger and more mesenchymal, typified by a spindle-shaped EMT phenotype (Fig. S6D). Additionally, Transwell assays demonstrated that the H1975-OR cells had significantly enhanced migration and invasion capabilities compared to the parental cells (Fig. S6E), providing functional evidence of altered cell behavior. The western blotting and immunofluorescence studies yielded similar results (Fig. 5D, E). Therefore, we concluded that EMT contributed to the acquired osimertinib resistance in these cells. The PDO1-OR model also exhibited significant EMT activation, which was confirmed through immunofluorescence experiments demonstrating downregulated E-cadherin and upregulated vimentin (Fig. 5F).

Whether RBM15 contributes to osimertinib resistance via the EMT mechanism was examined using paired RNA-seq data from eight patients who developed *EGFR*-TKI resistance [27]. We assessed the RBM15, CDH1, ZEB1, and AXL expression levels before treatment and at disease progression onset, and observed that increased RBM15 expression typically coincided with reduced CDH1 and increased ZEB1 and AXL (Fig. 5G–J). A comprehensive dataset evaluation to explore the relationships between RBM15 and these markers demonstrated that RBM15 expression negatively correlated with CDH1 and positively correlated with ZEB1 and AXL (Fig. S6G–I). Further investigations demonstrated that silencing *RBM15* in the H1975-OR and PDO1-OR cells decreased ZEB1 and TWIST1 and increased E-cadherin. The simultaneous knockdown of *SPOCK1* reversed these changes (Fig. 5K–M). These results proved that RBM15 facilitates osimertinib resistance through *SPOCK1*-mediated EMT-related mechanisms, highlighting the intricate molecular interplay in drug resistance development.

#### **EMT and RBM15 upregulation are early events in the evolution of osimertinib resistance**

The importance of EMT and RBM15 in the evolution of osimertinib resistance was explored by continuously treating H1975 cells with 1  $\mu$ M osimertinib for 20 days. This regimen enabled the isolation of H1975-DTPCs, which demonstrated enduring osimertinib resistance through multiple passages. The CCK-8 assay results revealed that the H1975-DTPCs had an  $IC_{50}$  of 3.84  $\mu$ M, significantly higher than the  $IC_{50}$  of 0.74  $\mu$ M in the parental cells (Fig. 6A), signaling a shift from sensitivity to resistance. In the parental H1975 cells, osimertinib inhibited *EGFR* phosphorylation and suppressed p-AKT. Contrastingly, p-*EGFR* was inhibited in the H1975-DTPCs, but p-AKT was not notably altered (Fig. 6B). Western blotting revealed that H1975-DTPCs expressed higher RBM15 levels and lower *SPOCK1* levels compared to their parental counterparts (Fig. 6C). Western blotting and immunofluorescence confirmed increased ZEB1 and vimentin expression and decreased E-cadherin in the H1975-DTPCs (Fig. 6D, E). These results indicated





that increased RBM15 expression, decreased SPOCK1 expression, and the emergence of EMT traits in DTPCs are early markers in the development of osimertinib resistance. Targeting RBM15 could potentially be used with osimertinib at the early treatment stages to extend the duration of TKI benefits.

## DISCUSSION

The array of RNA modifications is vast, and extensive research has established that m6A is the most prevalent modification within mRNA and non-coding RNA (ncRNA) [32–34]. m6A is implicated in various pre-translational regulatory mechanisms, including mRNA



**Fig. 4 SPOCK1 is a downstream target of RBM15, and reverses RBM15-induced osimertinib resistance.** **A** Venn diagrams were generated from the set of genes enriched for transcripts substantially altered after RBM15 silencing (RNA-seq) and the set of genes enriched for m6A-modified transcripts (m6A-seq). Sixteen genes were chosen based on overlap. **B** Top motif identified by HOMER with m6A-seq peaks. **C** Peak regions of m6A modifications detected by MeRIP-seq. **D, E** qRT-PCR was conducted to assess the differences in mRNA expression of the above 16 genes after RBM15 knockdown in H1975 and HCC827 cells. *T* test. **F, G** Western blot assessment of the correlation between RBM15 and SPOCK1 protein expression. **H, I** RIP-PCR validated RBM15 and m6A binding to *SPOCK1* mRNA. *T* test. **J** Changes in total RNA m6A modification levels after 48-h DAA treatment. *T* test. **K** Alteration of *SPOCK1* mRNA levels in H1975 cells and HCC827 cells after DAA treatment. *T* test. **L, M** Western blot and qRT-PCR demonstrated reduced SPOCK1 expression in H1975-OR cells and PDO1-OR. *T* test. **N** Osimertinib IC<sub>50</sub> value of H1975-OR cells transfected with si-NC, si-RBM15, or si-SPOCK1. *T* test. **O** Osimertinib IC<sub>50</sub> value of PDO1-OR transfected with sh-NC, sh-RBM15, or sh-SPOCK1. *T* test. **P, Q** Effects of RBM15 and SPOCK1 knockdown on H1975-OR and PDO1-OR apoptosis assessed using flow cytometry and TUNEL staining. *T* test. Error bars represent the means  $\pm$  SDs. \**P* < 0.05, \*\**P* < 0.01, \*\*\**P* < 0.001, \*\*\*\**P* < 0.0001.

stabilization, pre-mRNA splicing, and protein translation modification [35, 36]. A growing body of evidence supports the role of m6A in the etiology of various malignancies, including lung cancer, where alterations in WER expression alter m6A abundance [33, 37]. RBM15 is a writer that engages the methyltransferase complex and recruits WTAP–METTL3, directing the complex to target RNA and facilitate methylation [38]. RBM15 advances laryngeal squamous cell carcinoma progression through IGF2BP3-dependent modulation of TMBIM6 [12]. In castration-resistant prostate cancer, UBA1/RBM15-mediated attenuation of *TPM1* mRNA degradation promotes tumor proliferation and metastasis, enhancing the efficacy of docetaxel treatment [39]. Furthermore, RBM15 interacts with Circ-CTNNB1 to orchestrate m6A modification of hexokinase 2 (HK2), glucose-6-phosphate isomerase (GPI), and phosphoglycerate kinase 1 (PGK1), facilitating the glycolytic pathway and activating osteosarcoma [40].

Despite fewer studies in lung cancer, elevated RBM15 expression in lung cancer cells fosters cell proliferation, migration, and invasion [14, 41], while suppressing RBM15 induces ferroptosis via the TGF- $\beta$ –Smad2 pathway in these cells [14]. Our investigation used TCGA and THPA data and identified RBM15 as a m6A-WER with significant clinical potential in LUAD. Subsequent analyses using cell lines, tissue specimens, TMA cohorts, and PDOs confirmed that RBM15 is highly expressed in LUAD, highlighting its correlation with poor prognosis. Furthermore, we determined that inhibiting RBM15 decreased LUAD cell proliferation, migration, and invasion in vitro and in vivo, while overexpressing RBM15 yielded opposite effects. These results confirmed the indispensable role of RBM15 in LUAD and underscored its potential usefulness as a biomarker.

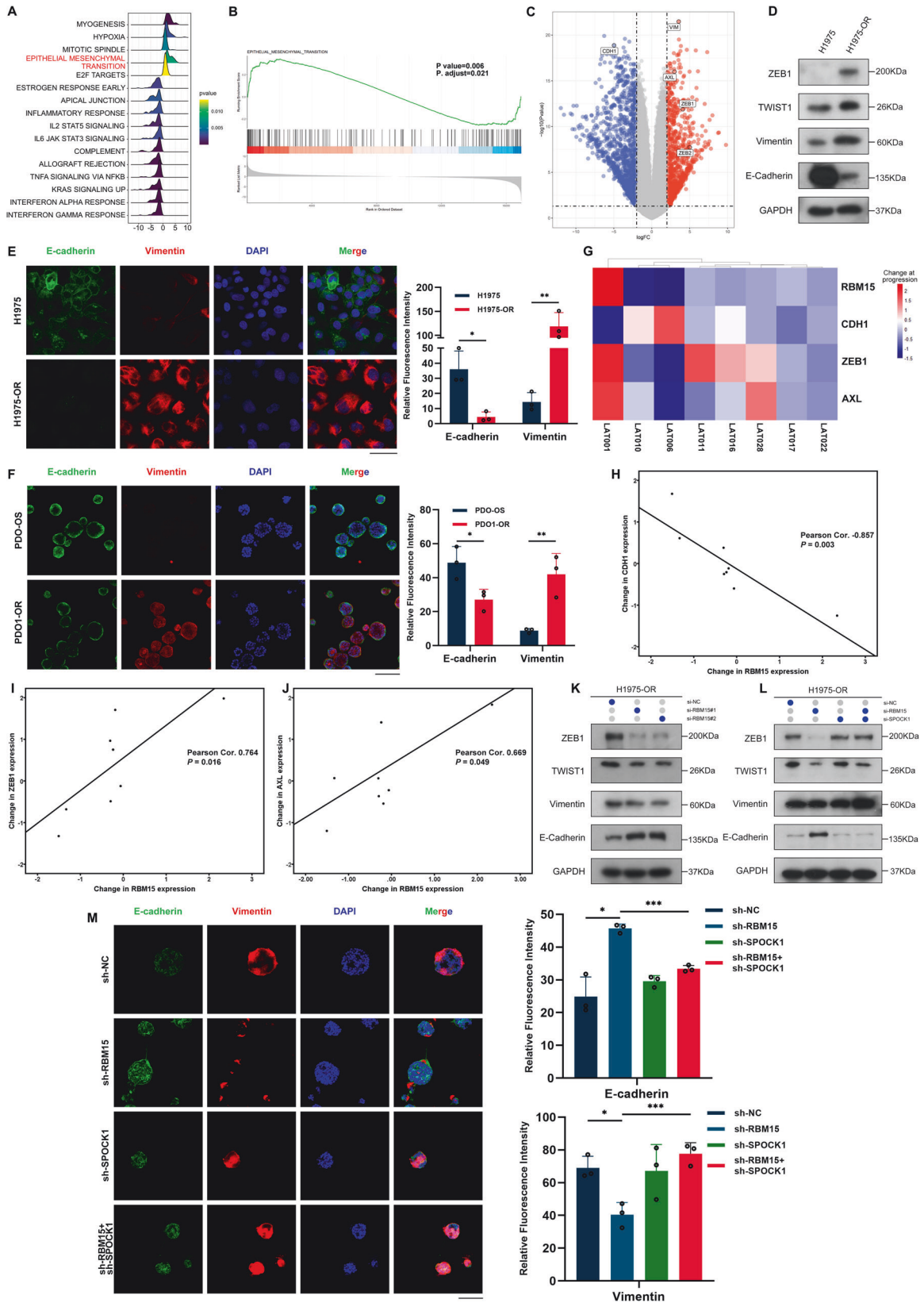
Examination of the correlation between RBM15 expression and clinical data from a TMA cohort revealed that patients harboring *EGFR* mutations exhibited elevated RBM15 expression levels, which was corroborated using PDO analyses. Furthermore, these patients, characterized by heightened RBM15 expression coupled with *EGFR* mutations, displayed reduced OS and PFS durations. However, no statistically significant association was observed between RBM15 expression and OS in patients without *EGFR* mutations. This suggested that RBM15 might have a particularly significant and pronounced role in *EGFR* mutations. Standard therapeutic regimens for patients with activating *EGFR* mutations, specifically exon 19 deletions (del19) and the L858R mutation, predominantly involve administering *EGFR*-TKIs [42]. Nonetheless, resistance invariably develops, mediated through *EGFR*-dependent and -independent mechanisms [43]. Building on these insights, we overexpressed RBM15 in HCC827 and NCI-H1975 cell lines, which substantially decreased osimertinib sensitivity. Subsequently, we established H1975-OR cells, in which RBM15 upregulation was identified as critical for AKT signaling activation and as an independent pathway activation apart from *EGFR*. Subsequent RBM15 knockdown in these cells increased drug responsiveness and intensified apoptotic responses following pharmacological intervention. The findings were aligned more closely with clinical outcomes by extending the study to include PDO1-OR and in vivo murine models, yielding consistent results. While the resistant

tumor microenvironment is significant in the evolution of TKI resistance, the aberrant upregulation of RBM15 observed in the resistant cell and organoid models underscores a pronounced cell-autonomous effect.

Subsequently, candidate genes that exhibited pronounced m6A modifications were identified using MeRIP-seq. Integrating these findings with RNA-seq and qRT-PCR analyses identified SPOCK1 as a putative downstream target of RBM15. RIP experiments coupled with rescue assays determined that RBM15 modulates the m6A landscape of *SPOCK1* mRNA, suppressing SPOCK1 expression and implicating it in the cellular mechanisms underlying osimertinib resistance. The *SPOCK1* gene encodes the core protein of a seminal plasma proteoglycan, which features chondroitin and heparan sulfate chains. While earlier research reported that SPOCK1 expression is elevated in osimertinib-resistant HCC827 and PC9 cell lines, fostering resistance to the drug [44], our studies revealed a contrary scenario where SPOCK1 expression was attenuated in resistant cells, displaying an inverse relationship with RBM15 levels. Intriguingly, depleting SPOCK1 expression reversed the enhanced osimertinib sensitivity triggered by RBM15 depletion. We conjecture that the discrepancies with previous findings may be attributed to: (1) genetic and phenotypic profile variability of the resistant cell lines used, notably the H1975-OR and PDO1-OR cells, which might differ from those in previous investigations; (2) the distinct immunological environments these resistant cells inhabit; (3) the particular resistance phenotypes these cells manifest. Such elements likely induce shifts in the gene regulatory networks, leading to varied outcomes. As earlier studies did not thoroughly explore the resistance mechanisms at the cellular level, identifying the precise origins of these discrepancies remains challenging.

Diverse mechanisms confer acquired osimertinib resistance, incorporating secondary *EGFR* mutations (e.g., C797S), MET amplification, and phenotypic cellular variations such as EMT and small cell transformation. Combined therapeutic strategies using osimertinib with MET or MEK inhibitors have been delineated to address MET amplification [45, 46]. However, resistance from EMT lacks specific therapeutic strategies; therefore, evading these resistant phenotypes is a critical challenge [47, 48]. In our study, H1975-OR cell WES identified *EGFR* L858R and T790M mutations, with no additional resistance-associated mutations detected. Subsequent RNA-seq and GSEA underscored the pronounced enrichment of EMT characteristics, including the dysregulated expression of EMT-associated genes. These results were validated using rigorous experimental evaluations in resistant cells, highlighting profound EMT-related alterations congruent with earlier observations of EMT in preclinical resistance models and clinical cases [49].

The results were extended to a clinical setting using paired analyses of genomic data from pre-treatment and initial post-progression tumor samples in eight patients with *EGFR*-mutant NSCLC. We focused on the dynamics of the EMT markers CDH1, ZEB1, and AXL, and the RBM15 expression shifts. The analysis revealed that tumors with significant EMT marker expression variability were strongly correlated with markedly altered RBM15



expression, providing clinical corroboration with our preclinical insights. Experimental validation demonstrated that knocking down RBM15 suppressed ZEB1 and TWIST1 and activated E-cadherin, which were reversed upon additional knockdown of

*SPOCK1*. These insights were corroborated in PDO1-OR that exhibited EMT phenotypes. However, previous studies have confirmed that *SPOCK1* promotes the metastasis of pancreatic cancer through NF- $\kappa$ B-dependent epithelial-mesenchymal

**Fig. 5 RBM15 confers osimertinib resistance in H1975-OR and PDO1-OR with the EMT phenotype.** **A, B** GSEA pathway enrichment was performed using DEGs. **C** Volcano plot of RNA-seq results displaying DEGs in H1975 and H1975-OR. **D, E** Western blot and immunofluorescence detection of protein expression of EMT-related indicators (scale bar: 50  $\mu$ m). **T** test. **F** Immunofluorescence detection of protein expression of EMT-related indicators in PDO-OS and PDO1-OR (scale bar: 25  $\mu$ m). **T** test. **G** Change in CDH1, ZEB1, AXL, and RBM15 expression in osimertinib refractory tissues and matched pre-treatment tissues. **H–J** Spearman's correlation of change in CDH1, ZEB1, AXL, and RBM15 expression in eight patients with matched pre- and post-osimertinib treatment. Pearson test. **K, L** Western blot and immunofluorescence assays reveal changes in protein expression of EMT indicators in H1975-OR and PDO1-OR after RBM15 knockdown. **M** Immunofluorescence assays reveal changes in protein expression of EMT indicators in PDO1-OR after RBM15 and SPOCK1 knockdown (scale bar: 50  $\mu$ m). **T** test. Error bars represent the means  $\pm$  SDs. \* $P$  < 0.05, \*\* $P$  < 0.01, \*\*\* $P$  < 0.001.

transition [50], and the activation of the SPOCK1-snail/slug axis in EMT also plays a role in facilitating the metastasis of prostate cancer [51]. These findings appear to contradict our conclusions. Nevertheless, the functions and mechanisms of SPOCK1 have not been fully explored, and it is not uncommon for the same molecule to exhibit opposing functions in different studies [52, 53], particularly when there are significant differences in tumor types and stages of development. Our experimental results provide strong evidence to support our conclusions. Overall, our results supported the strategic targeting of the RBM15–SPOCK1 axis in managing EMT-associated osimertinib resistance.

DTPCs are cells that endure beyond day 14 of pharmacological intervention. DTPCs might enter a reversible state of drug tolerance in response to therapeutic exposure and can re-initiate the cell cycle during ongoing drug treatment, forming a transiently drug-tolerant persistent cohort [54, 55]. Furthermore, clinically pertinent drug-resistant cancer cells might preexist or evolve from these drug-tolerant progenitors [56]. Following a 20-day osimertinib regimen, we successfully isolated the surviving H1975 cells and established the H1975-DTPCs. Notably, these cells demonstrated pronounced RBM15 upregulation coupled with significantly downregulated SPOCK1, increased ZEB1 and vimentin expression, and decreased E-cadherin expression. These alterations signify an early manifestation of resistance development post-osimertinib therapy initiation, underscored by the upregulated RBM15 and EMT markers and the downregulated SPOCK1. These observations supported the potential clinical efficacy of early intervention targeting the RBM15–SPOCK1 axis in managing osimertinib resistance.

Acquired EGFR-TKI resistance is often characterized by a pervasive resilience extending across a wide array of kinase inhibitors and demonstrating widespread acquired resistance [31]. Furthermore, the unsatisfactory outcomes associated with ICI treatment [20] underscore the urgent necessity for more effective therapeutic strategies. The substantial heterogeneity of tumors and the diverse mechanisms underlying resistance are the primary challenges in the management of osimertinib-resistant lung cancer [57]. Our result demonstrated that RBM15–SPOCK1 axis dysregulation precipitates the evolution of EMT-associated osimertinib resistance. Consequently, targeting the RBM15–SPOCK1 axis could be an effective early intervention strategy to overcome EGFR-TKI resistance (Fig. 6F).

Some key issues limit the translational applicability of our results. Primarily, the development and clinical deployment of RBM15-specific therapeutics necessitates further research. Furthermore, the absence of routine assessments of EMT and RBM15 expression before the emergence of resistance or at an earlier stage significantly restricts the potential for clinical verification of the mechanisms that foster EGFR-TKI resistance outlined in this study. Additionally, the intrinsic nature of EMT as a cellular phenotype alteration potentially modulated by the patient's tumor microenvironment and a spectrum of epigenetic controls adds substantial complexity to using EMT inhibition as a therapeutic strategy [58]. These factors highlight the intricate challenges in effectively translating these research insights into clinical practice.

## MATERIALS AND METHODS

### Patient samples

Forty LUAD samples and adjacent non-tumorous lung tissues were collected from the Department of Thoracic Surgery at Lihuili Hospital, Ningbo Medical Center. All patients had not received treatment prior to surgery and were histopathologically diagnosed with LUAD postoperatively. The Ethics Committee of Lihuili Hospital, Ningbo Medical Center, approved this study and all patients provided informed consent (KY2022PJ140). This study does not involve the extent of blinding.

### Cell culture

Human embryonic lung fibroblasts (MRC-5) were cultured in minimum essential medium (MEM; Gibco, MA, USA). The LUAD cell lines (HCC827, PC9, NCI-H1650, A549, NCI-H1975) were cultured in RPMI 1640 medium (Gibco). Both media were supplemented with 10% FBS (Pricella, Wuhan, China) and 1% penicillin/streptomycin (Beyotime, Shanghai, China). Routine mycoplasma detection and elimination were performed. Cell authentication was verified using short tandem repeat profiling.

### Construction of osimertinib-resistant cell lines

The osimertinib-resistant cell line (H1975-OR) derived from NCI-H1975 cells was acquired from MeisenCTCC (Zhejiang, China). Resistance in the parental NCI-H1975 cell line was induced by gradually increasing osimertinib concentrations. Briefly, log-phase cells underwent shock induction using a gradient concentration increase method, starting with 500 nM osimertinib. The drug was removed after 24-h treatment, and the drug shock was repeated once the cells resumed growth. The drug concentration was increased by 500 nM every 15 days. The cells were continuously cultured for 6–9 months. The resistance index (RI) was calculated as the  $IC_{50}$  of the resistant cells divided by the parental cell  $IC_{50}$ . An RI of 1–5 indicated low resistance, 5–15 indicated moderate resistance, and >15 indicated high resistance.

### Construction of osimertinib-tolerant cells

H1975 osimertinib DTPCs (H1975-DTPCs) were generated by continuously exposing the parental H1975 cells to 1  $\mu$ M osimertinib for 20 days. Subsequently, the cells were harvested, and their RNA and protein expression was analyzed using immunofluorescence, quantitative real-time PCR (qRT-PCR), and western blotting. The collected cells were then plated in 96-well plates for drug sensitivity testing.

### Patient-derived organoid (PDO) construction and culture

LUAD organoids were derived from biopsy samples collected from patients at their initial diagnosis, prior to treatment. Additionally, osimertinib-resistant organoids were established from lung puncture tissues obtained from patients whose tumors had progressed despite osimertinib treatment. Upon excision, the tissues were immediately transported to a level 2 biosafety laboratory (BSL-2) for the primary organoid construction. The tissues were minced, digested with enzymatic solutions, and filtered to collect single cells, which were cultured in Matrigel (Corning, NY, USA). The organoid density and morphology were monitored daily, with fresh culture medium replaced every 2–3 days. The primary organoids typically formed solid or cystic structures measuring 50–100  $\mu$ m within 2 weeks. The organoids could sustain ex vivo expansion and maintained stable morphology throughout the culture.

### Lentiviral construction and infection and small interfering RNA (siRNA)

Lentiviral systems for gene overexpression or knockdown were purchased from GeneChem (Shanghai, China), with the lentiviral vectors carrying



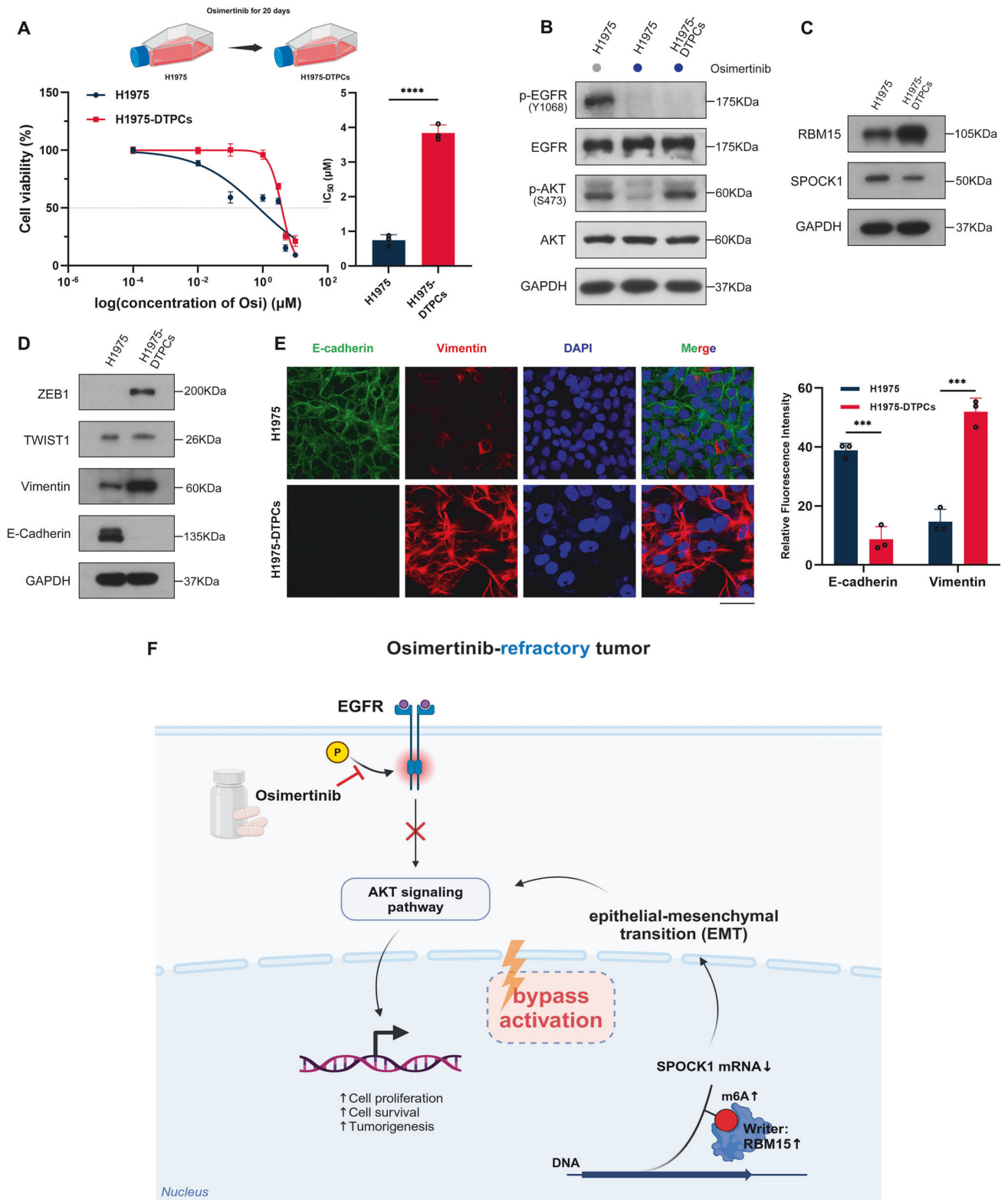


**Fig. 6** EMT induction and RBM15 upregulation as precursors to osimertinib resistance development. **A** H1975 cells were exposed to 1  $\mu\text{M}$  osimertinib and cultured for 20 days to select H1975-DTP cells (top panel). H1975 and H1975-DTP cells were incubated with osimertinib for 48 h, cell viability was measured using the CCK-8 assay, and the  $\text{IC}_{50}$  was calculated (bottom panel). *T* test. **B** Western blot investigation of EGFR, ERK, and AKT protein levels and their phosphorylation. **C** Western blot assessment of RBM15 protein expression levels in H1975 and H1975-DTPCs. **D**, **E** Western blot and immunofluorescence assessment of EMT marker proteins in H1975 and H1975-DTP cells (scale bar: 50  $\mu\text{m}$ ). *T* test. **F** A model diagram demonstrating that RBM15 suppresses *SPOCK1* mRNA expression through m6A modification, enhancing EMT-mediated osimertinib resistance in refractory tumors. This figure was created using the BioRender website (<https://biorender.com>). Error bars represent the means  $\pm$  SDs. \*\*\* $P < 0.001$ , \*\*\*\* $P < 0.0001$ .



puromycin or geneticin resistance markers. Before infection, the cells were seeded in 6-well plates. The negative controls were the corresponding empty lentiviral vectors. After 48-h infection, the cells were selected using puromycin or geneticin, and gene expression was validated using qRT-PCR and western blotting. The siRNAs were synthesized by GenePharma (Shanghai, China) and transfected into cells using Lipofectamine 2000 (Invitrogen, MA, USA). The cells were collected 48 h post-transfection for further experimentation. Tables S1 and S2 list the oligonucleotide sequences.

### Protein extraction and western blotting

The cells were lysed in radioimmunoprecipitation assay buffer (Beyotime) and centrifuged at 12,000 rpm for 15 min at 4 °C. The supernatant proteins were quantified using the bicinchoninic acid (BCA) method (Beyotime). An appropriate volume of SDS buffer was added according to the protein concentration, and the samples were heated in a 100 °C bath for 5 min, then cooled on ice for electrophoresis. Proteins were separated using SDS-PAGE and transferred to PVDF membranes. The membranes were blocked with 5% skimmed milk or 1% bovine serum albumin (BSA) and sequentially incubated with primary antibodies and horseradish peroxidase-conjugated secondary antibodies (Cell Signaling Technology, MA, USA). Protein bands were detected using enhanced chemiluminescence reagents (Advansta, CA, USA) under dark conditions. Table S3 lists the antibodies used.

### qRT-PCR

RNA was extracted using TRIzol (Takara, Japan). A PrimeScript RT reagent kit and TB GREEN PriMix (Takara) were used for the reverse transcription and qRT-PCR, respectively. mRNA expression was quantified using a LightCycler 480II system (Roche, Switzerland). The expression data were analyzed using the comparative threshold cycle ( $2^{-\Delta\Delta C_t}$ ) method. Table S4 lists the primer sequences used.

### Tissue microarray (TMA), immunohistochemistry (IHC), and TUNEL assay

A LUAD tissue microarray chip containing 98 LUAD tissues and 82 adjacent non-cancerous tissues collected from patients between July 2004 and June 2009 was obtained from Shanghai Outdo Biotech Company (Shanghai, China). The samples were sourced from the National Human Genetic Resources Sharing Service Platform and ethically reviewed by the Shanghai Outdo Biotech Company Ethics Committee (SHYJS-CP-1904014). All experiments were conducted in compliance with relevant guidelines. Informed consent was obtained from all patients.

For the IHC experiments and TMA, animal tissue sections and organoid sections were dewaxed and underwent antigen retrieval, followed by incubation with the appropriate antibodies or TUNEL staining using a cell death detection fluorescein kit (Invitrogen). Imaging was performed using an Aperio scanner for microarrays or an inverted fluorescence microscope (Nikon, Japan). A semi-quantitative evaluation was conducted based on staining intensity and the positive staining percentage. Staining intensity was categorized into 1 (weak positive), 2 (moderate positive), and 3 (strong positive). The percentage of positive cells was classified into 1 (0–10%), 2 (11–50%), 3 (51–80%), or 4 (81–100%). The final score was the product of the staining intensity and percentage of positive cells.

### Immunofluorescence

The cells were fixed for 20 min in 4% paraformaldehyde, washed three times with PBS, and permeabilized with 0.2% Triton X-100 for 15 min. After blocking with BSA, the cells were sequentially incubated with primary and secondary antibodies (Invitrogen). Subsequently, the nuclei were stained for 5 min using DAPI. Fluorescent imaging was conducted using a laser scanning confocal microscope (Zeiss, Germany). Table S3 details the antibodies used.

### m6A RNA methylation quantification

m6A levels were quantitatively analyzed using an Abcam m6A RNA Methylation Assay Kit (Abcam, ab185912, UK) according to the manufacturer's instructions. The RNA was bound, capturing m6A RNA, and the signal was detected. Absorbance was measured at 450 nm. The m6A levels were calculated based on the negative and positive controls.

### Cell proliferation and drug sensitivity assays

For the cell proliferation assay, 5000 cells per well were seeded in a 96-well plate. A 1:9 dilution of Cell Counting Kit-8 (CCK-8, APExBio, Houston, USA)

solution was added at 0, 24, 48, and 72 h, and the absorbance at 450 nm was measured after incubation at 37 °C. For the drug sensitivity assay, 5000 cells per well were seeded in a 96-well plate and treated for 48 h with osimertinib before a 1:9 diluted CCK-8 solution was added. Absorbance at 450 nm was measured following incubation at 37 °C. The  $IC_{50}$ , representing (the osimertinib concentration required to inhibit cell growth by 50%), was calculated using non-linear regression analysis of dose–response data using GraphPad Prism 9.0 (CA, USA).

### EdU assay

Cells were seeded at a density of 5000 cells per well in a 96-well plate and, upon reaching 80% confluence, were fixed with 4% paraformaldehyde for 20 min. After three PBS washes, the proliferating cells were labeled using a Click-iT EdU Alexa Fluor 488 Imaging Kit (Invitrogen, C10337). Subsequently, the nuclei were stained for 5 min using DAPI, and the cells were imaged under a fluorescence microscope (EVOS M7000, Invitrogen).

### Transwell assay

Cell proliferation and migration were assessed by seeding 200  $\mu$ l single-cell suspension containing 50,000 cells in serum-free medium into the upper Transwell chamber, while 700  $\mu$ l medium containing 10% FBS was added to the lower chamber. The cells were allowed to migrate for a specified duration in an incubator, then fixed in 4% paraformaldehyde. Following PBS washing, the cells were stained for 15 min with crystal violet. Non-migrating/non-invading cells in the upper chamber were wiped away before imaging under a microscope.

### Flow cytometry

Apoptosis was assessed using an Annexin V/fluorescein isothiocyanate (FITC) and propidium iodide (PI) assay kit (Multisciences, Zhejiang, China) according to the manufacturer's protocol. The apoptosis rates in the cell groups were determined using flow cytometry (BD FACSCanto, NJ, USA). The data were analyzed using FlowJo 10.8.1 (Tree Star, OR, USA).

### Methylated RNA immunoprecipitation sequencing (MeRIP-seq)

RNA was extracted, purified, and fragmented into ~100 nucleotide segments using a Magna MeRIP m6A Kit (Millipore, 17-10499, MA, USA). m6A-modified mRNA fragments were enriched using m6A antibody-coated immunomagnetic beads. The complexes were separated, and the enriched RNA was reverse-transcribed into cDNA, which was used for library construction. Sequencing was performed on the Illumina NovaSeq™ 6000 platform with the PE150 sequencing mode. The sequencing services and data analysis were by Hangzhou Kaitai Biotechnology Co., Ltd. (Hangzhou, China).

### RNA sequencing (RNA-seq)

The extracted total RNA underwent RNA sample testing, library construction, and library quality control, followed by PE150 sequencing on the Illumina NovaSeq 6000. The sequencing services and data analysis were by Hangzhou Kaitai Biotechnology Co., Ltd.

### Immunoprecipitation (IP)

The cells were lysed for 2 h on ice using IP lysis buffer (Beyotime). The protein lysate was centrifuged at 12,000 rpm for 15 min and divided into Input, IP, and IgG aliquots. The protein lysates were incubated with Protein A/G agarose beads pre-bound with antibodies. After washing, the immunoprecipitated protein complexes were separated from the agarose beads, and the RBM15-associated proteins were detected using immunoblots.

### RNA immunoprecipitation (RIP)

The RIP assay was conducted using a Magna RIP Kit (17-700, Millipore) according to the kit protocol. Briefly, magnetic beads pre-bound with anti-RBM15 antibody (Proteintech, 66059-1-Ig, IL, USA) or mouse IgG were added to an adequate amount of cell lysate and incubated overnight at 4 °C with rotation. The proteins were digested using protease, and RNA was extracted and purified using TRIzol, followed by reverse transcription into cDNA. The cDNA was analyzed using qRT-PCR.

### Methylation inhibitor treatment

The cells were treated for 48 h with 0, 100, or 200  $\mu$ M 3-deazaadenosine (DAA, APExBio, B8470). Subsequently, RNA was harvested and extracted for qRT-PCR analysis.

## In vivo tumorigenesis assay

Xenograft models were established using stably transfected H1975 cells and H1975-OR cells with short hairpin RNA negative control (sh-NC), sh-RBM15, and sh-SPOCK1. Male nude mice (4 weeks old) were injected subcutaneously on the right flank with  $2 \times 10^5$  cells. When the tumors reached a longitudinal diameter of 5 mm, the mice were randomly assigned to each group and subsequently treated orally with an equal volume of osimertinib mesylate (Selleck, S5078, TX, 20 mg/kg/day) or corn oil by gavage every 2 days. The tumor dimensions were measured twice daily. The tumor volume was calculated as follows:  $(\text{length} \times \text{width}^2)/2$ . The First Affiliated Hospital of Zhejiang University Ethics Committee approved the animal study protocol (2024-1219). All mice were housed in a pathogen-free environment with controlled temperature, maintained on a 12-h light/dark cycle, and had ad libitum access to food and water. Each group comprised at least six animals. Mice that did not develop tumors by 30 days post-subcutaneous injection were excluded from the study. This study does not involve the extent of blinding.

## Statistical analysis

All experiments were independently repeated three times. The statistical methods for analyzing database data and clinical samples were determined based on the underlying assumptions and variability. When the variances between the two groups were similar, the Student's *t*-test was used; otherwise, the Mann–Whitney test was employed. Data from cell cultures, organoids, and in vivo experiments were analyzed using Student's *t*-test. The results are presented as the mean  $\pm$  SD. Survival analysis was conducted using the Kaplan–Meier method; significance was tested using the log-rank test. All statistical analyses were performed using SPSS 21.0 (IBM, NY, USA). Graphs were created using SPSS 21.0 and GraphPad Prism 9.0.  $P < 0.05$  was considered statistically significant.

## DATA AVAILABILITY

The data generated in this study are available upon request from the corresponding author.

## REFERENCES

- Sung H, Ferlay J, Siegel RL, Laversanne M, Soerjomataram I, Jemal A, et al. Global cancer statistics 2020: GLOBOCAN estimates of incidence and mortality worldwide for 36 cancers in 185 countries. *CA Cancer J Clin*. 2021;71:209–49. <https://doi.org/10.3322/caac.21660>.
- Byers LA, Diao L, Wang J, Saintigny P, Girard L, Peyton M, et al. An epithelial-mesenchymal transition gene signature predicts resistance to EGFR and PI3K inhibitors and identifies Axl as a therapeutic target for overcoming EGFR inhibitor resistance. *Clin Cancer Res*. 2013;19:279–90. <https://doi.org/10.1158/1078-0432.CCR-12-1558>.
- DeSantis CE, Miller KD, Goding Sauer A, Jemal A, Siegel RL. Cancer statistics for African Americans, 2019. *CA Cancer J Clin*. 2019;69:211–33. <https://doi.org/10.3322/caac.21555>.
- Desrosiers R, Friderici K, Rottman F. Identification of methylated nucleosides in messenger RNA from Novikoff hepatoma cells. *Proc Natl Acad Sci USA*. 1974;71:3971–5. <https://doi.org/10.1073/pnas.71.10.3971>.
- An Y, Duan H. The role of m6A RNA methylation in cancer metabolism. *Mol Cancer*. 2022;21:14. <https://doi.org/10.1186/s12943-022-01500-4>.
- An X, Wu W, Yang L, Dong J, Liu B, Guo J, et al. ZBTB7C m6A modification incurred by METTL3 aberration promotes osteosarcoma progression. *Transl Res*. 2023;259:62–71. <https://doi.org/10.1016/j.trsl.2023.04.005>.
- Liu T, Wei Q, Jin J, Luo Q, Liu Y, Yang Y, et al. The m6A reader YTHDF1 promotes ovarian cancer progression via augmenting EIF3C translation. *Nucleic Acids Res*. 2020;48:3816–31. <https://doi.org/10.1093/nar/gkaa048>.
- Han J, Wang JZ, Yang X, Yu H, Zhou R, Lu HC, et al. METTL3 promote tumor proliferation of bladder cancer by accelerating pri-miR221/222 maturation in m6A-dependent manner. *Mol Cancer*. 2019;18:110. <https://doi.org/10.1186/s12943-019-1036-9>.
- Shi J, Zhang Q, Yin X, Ye J, Gao S, Chen C, et al. Stabilization of IGF2BP1 by USP10 promotes breast cancer metastasis via CPT1A in an m6A-dependent manner. *Int J Biol Sci*. 2023;19:449–64. <https://doi.org/10.7150/ijbs.76798>.
- Zhou H, Yin K, Zhang Y, Tian J, Wang S. The RNA m6A writer METTL14 in cancers: Roles, structures, and applications. *Biochim Biophys Acta Rev Cancer*. 2021;1876:188609. <https://doi.org/10.1016/j.bbcan.2021.188609>.
- Hiriart E, Gruffat H, Buisson M, Mikaelian I, Keppler S, Meresse P, et al. Interaction of the Epstein-Barr virus mRNA export factor EB2 with human Spen proteins SHARP, OTT1, and a novel member of the family, OTT3, links Spen proteins with splicing regulation and mRNA export. *J Biol Chem*. 2005;280:36935–45. <https://doi.org/10.1074/jbc.M501725200>.
- Wang X, Tian L, Li Y, Wang J, Yan B, Yang L, et al. RBM15 facilitates laryngeal squamous cell carcinoma progression by regulating TM6IM6 stability through IGF2BP3 dependent. *J Exp Clin Cancer Res*. 2021;40:80. <https://doi.org/10.1186/s13046-021-01871-4>.
- Dong H, Zhang H, Mao X, Xu W, Zhang Y. RBM15 promotes the proliferation, migration and invasion of pancreatic cancer cell lines. *Cancers*. 2023;15. <https://doi.org/10.3390/cancers15041084>.
- Feng J, Li Y, He F, Zhang F. RBM15 silencing promotes ferroptosis by regulating the TGF-beta/Smad2 pathway in lung cancer. *Environ Toxicol*. 2023;38:950–61. <https://doi.org/10.1002/tox.23741>.
- Shigematsu H, Lin L, Takahashi T, Nomura M, Suzuki M, Wistuba II, et al. Clinical and biological features associated with epidermal growth factor receptor gene mutations in lung cancers. *J Natl Cancer Inst*. 2005;97:339–46. <https://doi.org/10.1093/jnci/dji055>.
- Ramalingam SS, Vansteenkiste J, Planchard D, Cho BC, Gray JE, Ohe Y, et al. Overall survival with osimertinib in untreated, EGFR-mutated advanced NSCLC. *N Engl J Med*. 2020;382:41–50. <https://doi.org/10.1056/NEJMoa1913662>.
- Rosell R, Carcereny E, Gervais R, Vergnenegre A, Massuti B, Felip E, et al. Erlotinib versus standard chemotherapy as first-line treatment for European patients with advanced EGFR mutation-positive non-small-cell lung cancer (EURTAC): a multicentre, open-label, randomised phase 3 trial. *Lancet Oncol*. 2012;13:239–46. [https://doi.org/10.1016/S1470-2045\(11\)70393-X](https://doi.org/10.1016/S1470-2045(11)70393-X).
- Li D, Ambrogio L, Shimamura T, Kubo S, Takahashi M, Chirieac LR, et al. BIBW2992, an irreversible EGFR/HER2 inhibitor highly effective in preclinical lung cancer models. *Oncogene*. 2008;27:4702–11. <https://doi.org/10.1038/nc.2008.109>.
- Sharma SV, Bell DW, Settleman J, Haber DA. Epidermal growth factor receptor mutations in lung cancer. *Nat Rev Cancer*. 2007;7:169–81. <https://doi.org/10.1038/nrc2088>.
- Piper Vallillo AJ, Viray H, Feldman J, Rangachari D. Management of treatment resistance in patients with advanced epidermal growth factor receptor-mutated lung cancer: personalization, parsimony, and partnership. *J Clin Oncol*. 2024;42:1215–21. <https://doi.org/10.1200/JCO.23.02417>.
- Leonetti A, Sharma S, Minari R, Perego P, Giovannetti E, Tiseo M. Resistance mechanisms to osimertinib in EGFR-mutated non-small cell lung cancer. *Br J Cancer*. 2019;121:725–37. <https://doi.org/10.1038/s41416-019-0573-8>.
- Thress KS, Pawelczak CP, Felip E, Cho BC, Stetson D, Dougherty B, et al. Acquired EGFR C797S mutation mediates resistance to AZD9291 in non-small cell lung cancer harboring EGFR T790M. *Nat Med*. 2015;21:560–2. <https://doi.org/10.1038/nm.3854>.
- Wu YL, Zhang L, Kim DW, Liu X, Lee DH, Yang JC, et al. Phase Ib/II study of capmatinib (INC280) plus gefitinib after failure of epidermal growth factor receptor (EGFR) inhibitor therapy in patients with EGFR-mutated, MET factor-dysregulated non-small-cell lung cancer. *J Clin Oncol*. 2018;36:3101–9. <https://doi.org/10.1200/JCO.2018.77.7326>.
- Zhu X, Zhou C, Zhao S, Zheng Z. Role of m6A methylation in retinal diseases. *Exp Eye Res*. 2023;231:109489. <https://doi.org/10.1016/j.exer.2023.109489>.
- Li Y, Gao X, Ni C, Zhao B, Cheng X. The application of patient-derived organoid in the research of lung cancer. *Cell Oncol*. 2023;46:503–19. <https://doi.org/10.1007/s13402-023-00771-3>.
- Giardiello F, Hirsch FR, Pirker R, Felip E, Valencia C, Smit EF. The role of anti-EGFR therapies in EGFR-TKI-resistant advanced non-small cell lung cancer. *Cancer Treat Rev*. 2024;122:102664. <https://doi.org/10.1016/j.ctrv.2023.102664>.
- Roper N, Brown AL, Wei JS, Pack S, Trindade C, Kim C, et al. Clonal evolution and heterogeneity of osimertinib acquired resistance mechanisms in EGFR mutant lung cancer. *Cell Rep Med*. 2020;1. <https://doi.org/10.1016/j.xcrm.2020.100007>.
- Maeser D, Gruener RF, Huang RS. oncoPredict: an R package for predicting in vivo or cancer patient drug response and biomarkers from cell line screening data. *Brief Bioinform*. 2021;22. <https://doi.org/10.1093/bib/bbab260>.
- Fu K, Xie F, Wang F, Fu L. Therapeutic strategies for EGFR-mutated non-small cell lung cancer patients with osimertinib resistance. *J Hematol Oncol*. 2022;15:173. <https://doi.org/10.1186/s13045-022-01391-4>.
- Zhang X, Maity TK, Ross KE, Qi Y, Cultraro CM, Bahta M, et al. Alterations in the global proteome and phosphoproteome in third generation EGFR TKI resistance reveal drug targets to circumvent resistance. *Cancer Res*. 2021;81:3051–66. <https://doi.org/10.1158/0008-5472.CAN-20-2435>.
- Nilsson MB, Sun H, Robichaux J, Pfeifer M, McDermott U, Travers J, et al. A YAP/FOXO1 axis mediates EMT-associated EGFR inhibitor resistance and increased expression of spindle assembly checkpoint components. *Sci Transl Med*. 2020;12. <https://doi.org/10.1126/scitranslmed.aaz4589>.
- Wen S, Wei Y, Zen C, Xiong W, Niu Y, Zhao Y. Long non-coding RNA NEAT1 promotes bone metastasis of prostate cancer through N6-methyladenosine. *Mol Cancer*. 2020;19:171. <https://doi.org/10.1186/s12943-020-01293-4>.

33. Zaccara S, Ries RJ, Jaffrey SR. Reading, writing and erasing mRNA methylation. *Nat Rev Mol Cell Biol*. 2019;20:608–24. <https://doi.org/10.1038/s41580-019-0168-5>.
34. Wang X, Lu Z, Gomez A, Hon GC, Yue Y, Han D, et al. N6-methyladenosine-dependent regulation of messenger RNA stability. *Nature*. 2014;505:117–20. <https://doi.org/10.1038/nature12730>.
35. Song P, Yang F, Jin H, Wang X. The regulation of protein translation and its implications for cancer. *Signal Transduct Target Ther*. 2021;6:68. <https://doi.org/10.1038/s41392-020-00444-9>.
36. Alarcon CR, Lee H, Goodarzi H, Halberg N, Tavazoie SF. N6-methyladenosine marks primary microRNAs for processing. *Nature*. 2015;519:482–5. <https://doi.org/10.1038/nature14281>.
37. Huang H, Weng H, Chen J. m(6A) modification in coding and non-coding RNAs: roles and therapeutic implications in cancer. *Cancer Cell*. 2020;37:270–88. <https://doi.org/10.1016/j.ccell.2020.02.004>.
38. Patil DP, Chen CK, Pickering BF, Chow A, Jackson C, Guttman M, et al. m(6A) RNA methylation promotes XIST-mediated transcriptional repression. *Nature*. 2016;537:369–73. <https://doi.org/10.1038/nature19342>.
39. Wang H, Liu J, Zhu X, Yang B, He Z, Yao X. AZGP1P2/UBA1/RBM15 cascade mediates the fate determinations of prostate cancer stem cells and promotes therapeutic effect of docetaxel in castration-resistant prostate cancer via TPM1 m6A modification. *Research*. 2023;6:0252. <https://doi.org/10.34133/research.0252>.
40. Yang F, Liu Y, Xiao J, Li B, Chen Y, Hu A, et al. Circ-CTNNB1 drives aerobic glycolysis and osteosarcoma progression via m6A modification through interacting with RBM15. *Cell Prolif*. 2023;56:e13344. <https://doi.org/10.1111/cpr.13344>.
41. Ma M, Wang W, Li L, Wang X, Huang Q, Zhou C, et al. RBM15 facilitates lung adenocarcinoma cell progression by regulating RASSF8 stability through N6 Methyladenosine modification. *Transl Oncol*. 2024;46:102018. <https://doi.org/10.1016/j.tranon.2024.102018>.
42. Park K, Tan EH, O'Byrne K, Zhang L, Boyer M, Mok T, et al. Afatinib versus gefitinib as first-line treatment of patients with EGFR mutation-positive non-small-cell lung cancer (LUX-Lung 7): a phase 2B, open-label, randomised controlled trial. *Lancet Oncol*. 2016;17:577–89. [https://doi.org/10.1016/S1470-2045\(16\)30033-X](https://doi.org/10.1016/S1470-2045(16)30033-X).
43. Wu SG, Shih JY. Management of acquired resistance to EGFR TKI-targeted therapy in advanced non-small cell lung cancer. *Mol Cancer*. 2018;17:38. <https://doi.org/10.1186/s12943-018-0777-1>.
44. Gao Y, Yu M, Ma M, Zhuang Y, Qiu X, Zhao Q, et al. SPOCK1 contributes to the third-generation EGFR tyrosine kinase inhibitors resistance in lung cancer. *J Cell Biochem*. 2019;120:12566–73. <https://doi.org/10.1002/jcb.28523>.
45. Girard N. New strategies and novel combinations in EGFR TKI-resistant non-small cell lung cancer. *Curr Treat Options Oncol*. 2022;23:1626–44. <https://doi.org/10.1007/s11864-022-01022-7>.
46. Wang Q, Yang S, Wang K, Sun SY. MET inhibitors for targeted therapy of EGFR TKI-resistant lung cancer. *J Hematol Oncol*. 2019;12:63. <https://doi.org/10.1186/s13045-019-0759-9>.
47. Zhu X, Chen L, Liu L, Niu X. EMT-mediated acquired EGFR-TKI resistance in NSCLC: mechanisms and strategies. *Front Oncol*. 2019;9:1044. <https://doi.org/10.3389/fonc.2019.01044>.
48. Jakobsen KR, Demuth C, Sorensen BS, Nielsen AL. The role of epithelial to mesenchymal transition in resistance to epidermal growth factor receptor tyrosine kinase inhibitors in non-small cell lung cancer. *Transl Lung Cancer Res*. 2016;5:172–82. <https://doi.org/10.21037/tlcr.2016.04.07>.
49. Sequist LV, Waltman BA, Dias-Santagata D, Digumarthy S, Turke AB, Fidias P, et al. Genotypic and histological evolution of lung cancers acquiring resistance to EGFR inhibitors. *Sci Transl Med*. 2011;3:75ra26. <https://doi.org/10.1126/scitranslmed.3002003>.
50. Cui X, Wang Y, Lan W, Wang S, Cui Y, Zhang X, et al. SPOCK1 promotes metastasis in pancreatic cancer via NF-kappaB-dependent epithelial-mesenchymal transition by interacting with IkappaB-alpha. *Cell Oncol*. 2022;45:69–84. <https://doi.org/10.1007/s13402-021-00652-7>.
51. Chien MH, Lin YW, Wen YC, Yang YC, Hsiao M, Chang JL, et al. Targeting the SPOCK1-snail/slug axis-mediated epithelial-to-mesenchymal transition by apigenin contributes to repression of prostate cancer metastasis. *J Exp Clin Cancer Res*. 2019;38:246. <https://doi.org/10.1186/s13046-019-1247-3>.
52. Chen M, Zou C, Tian Y, Li W, Li Y, Zhang D. An integrated ceRNA network identifies miR-375 as an upregulated miRNA playing a tumor suppressive role in aggressive prostate cancer. *Oncogene*. 2024;43:1594–607. <https://doi.org/10.1038/s41388-024-03011-6>.
53. Li Q, Liu B, Chao HP, Ji Y, Lu Y, Mehmood R, et al. LRIG1 is a pleiotropic androgen receptor-regulated feedback tumor suppressor in prostate cancer. *Nat Commun*. 2019;10:5494. <https://doi.org/10.1038/s41467-019-13532-4>.
54. Nilsson MB, Yang Y, Heeke S, Patel SA, Potete A, Udagawa H, et al. CD70 is a therapeutic target upregulated in EMT-associated EGFR tyrosine kinase inhibitor resistance. *Cancer Cell*. 2023;41:340–355.e346. <https://doi.org/10.1016/j.ccell.2023.01.007>.
55. Oren Y, Tsabar M, Cuoco MS, Amir-Zilberstein L, Cabanos HF, Hutter JC, et al. Cycling cancer persister cells arise from lineages with distinct programs. *Nature*. 2021;596:576–82. <https://doi.org/10.1038/s41586-021-03796-6>.
56. Hata AN, Niederst MJ, Archibald HL, Gomez-Caraballo M, Siddiqui FM, Mulvey HE, et al. Tumor cells can follow distinct evolutionary paths to become resistant to epidermal growth factor receptor inhibition. *Nat Med*. 2016;22:262–9. <https://doi.org/10.1038/nm.4040>.
57. Passaro A, Janne PA, Mok T, Peters S. Overcoming therapy resistance in EGFR-mutant lung cancer. *Nat Cancer*. 2021;2:377–91. <https://doi.org/10.1038/s43018-021-00195-8>.
58. Soucheray M, Capelletti M, Pulido I, Kuang Y, Paweletz CP, Becker JH, et al. Intratumoral heterogeneity in EGFR-mutant NSCLC results in divergent resistance mechanisms in response to EGFR tyrosine kinase inhibition. *Cancer Res*. 2015;75:4372–83. <https://doi.org/10.1158/0008-5472.CAN-15-0377>.

## ACKNOWLEDGEMENTS

This work was supported by funding awarded to GX from Zhejiang Province Medical and Health Project (2022KY296), Ningbo Youth Science and Technology Innovation Leading Talents Program (2023QL054), Key R&D projects of Zhejiang Province [2024C03277(SD2)]; funding awarded to XC from the National Natural Science Foundation of China (82073191), the Innovative Research Team of High-level Local Universities in Shanghai (SHSMU-ZLXC20212302), and the Clinical Research Plan of SHDC (SHDC2022CRD025); funding awarded to WC from the Zhejiang Provincial Natural Science Foundation of China (LR20H160001) and the Key R&D Projects of Zhejiang Province (2020C03G5263593); funding awarded to HL from the Innovative Research Projects for Postgraduate Students of Ningbo University (Y202353350); and funding awarded to WS from the Ningbo Health Technology Project (2022Y53).

## AUTHOR CONTRIBUTIONS

HL and YL completed the study design, experimental operations, and manuscript writing. WC, XC, and GX provided funding support, manuscript review, and revisions. XZ and SZ participated in experimental design and method optimization. FC primarily conducted the bioinformatics data analysis and processing for the paper. SX and YM were involved in data verification and validation. WS, JT, and HC assisted with data collection and management. ZH, JZ, and KQ contributed to sample processing and preservation, as well as literature search assistance. All authors read and approved the final paper.

## COMPETING INTERESTS

The authors declare no competing interests.

## ADDITIONAL INFORMATION

**Supplementary information** The online version contains supplementary material available at <https://doi.org/10.1038/s41388-024-03220-z>.

**Correspondence** and requests for materials should be addressed to Wei Chen, Xinghua Cheng or Guodong Xu.

**Reprints and permission information** is available at <http://www.nature.com/reprints>

**Publisher's note** Springer Nature remains neutral with regard to jurisdictional claims in published maps and institutional affiliations.



**Open Access** This article is licensed under a Creative Commons Attribution-NonCommercial-NoDerivatives 4.0 International License, which permits any non-commercial use, sharing, distribution and reproduction in any medium or format, as long as you give appropriate credit to the original author(s) and the source, provide a link to the Creative Commons licence, and indicate if you modified the licensed material. You do not have permission under this licence to share adapted material derived from this article or parts of it. The images or other third party material in this article are included in the article's Creative Commons licence, unless indicated otherwise in a credit line to the material. If material is not included in the article's Creative Commons licence and your intended use is not permitted by statutory regulation or exceeds the permitted use, you will need to obtain permission directly from the copyright holder. To view a copy of this licence, visit <http://creativecommons.org/licenses/by-nc-nd/4.0/>.

© The Author(s) 2024